Local density of electromagnetic states within a nanometric gap formed between two thin films supporting surface phonon polaritons

Mathieu Francoeur,[1,a)] M. Pinar Mengüç,[1,2,a)] and Rodolphe Vaillon[3,b)]
[1]*Department of Mechanical Engineering, Radiative Transfer Laboratory, University of Kentucky, Lexington, Kentucky 40506-0503, USA*
[2]*Ozyegin University, Altunizade, Uskudar, 34662 Istanbul, Turkey*
[3]*CNRS, INSA-Lyon, UCBL, CETHIL, Université de Lyon, UMR5008, F-69621 Villeurbanne, France*

(Received 24 June 2009; accepted 15 December 2009; published online 9 February 2010)

We present a detailed physical analysis of the near-field thermal radiation spectrum emitted by a silicon carbide (SiC) film when another nonemitting SiC layer is brought in close proximity. This is accomplished via the calculation of the local density of electromagnetic states (LDOS) within the gap formed between the two thin films. An analytical expression for the LDOS is derived, showing explicitly that (i) surface phonon polariton (SPhP) coupling between the layers leads to four resonant modes, and (ii) near-field thermal radiation emission is enhanced due to the presence of the nonemitting film. We study the impact of the interfilm separation gap, the distance where the fields are calculated, and the thickness of the nonemitting layer on the spectral distribution of the LDOS. Results show that for an interfilm gap of 10 nm, the near-field spectrum emitted around the SPhP resonance can increase more than an order of magnitude as compared to a single emitting thin layer. Interfilm SPhP coupling also induces a loss of spectral coherence of resonance, mostly affecting the low frequency modes. The effect of the nonemitting film can be observed on LDOS profiles when the distance where the fields are calculated is close to the interfilm gap. As the LDOS is calculated closer to the emitter, the near-field spectrum is dominated by SPhPs with small penetration depths that do not couple with the modes associated with the nonemitting film, such that thermal emission is similar to what is observed for a single emitting layer. Spectral distribution of LDOS is also significantly modified by varying the thickness of the nonemitting film relative to the thickness of the emitting layer, due to an increasing mismatch between the cross-coupled SPhP modes. The results presented here show clearly that the resonant modes of thermal emission by a polar crystal can be enhanced and tuned, between the transverse and longitudinal optical phonon frequencies, by simply varying the structure of the system. This analysis provides the physical grounds to tune near-field thermal radiation emission via multilayered structures, which can find application in nanoscale-gap thermophotovoltaic power generation. © *2010 American Institute of Physics*.
[doi:10.1063/1.3294606]

I. INTRODUCTION

Near-field radiative heat transfer by and between bulk materials was extensively studied over the past years. On the other hand, attention was paid only recently to near-field thermal radiation emission by nanometric films supporting surface waves.[1–8] When the emitter of thermal radiation is thin, surface waves associated with each interface couple within the layer and split the single resonance into antisymmetric and symmetric modes, a phenomenon that was investigated in the past for both surface phonon polaritons (SPhPs) and surface plasmon polaritons (SPPs).[9–16] This resonance splitting affects the spectrum emitted and can thus be used to tune near-field thermal radiation emission; such control over the near-field spectrum emitted can find application in nanoscale-gap thermophotovoltaic (TPV) power generation.[17,18]

Biehs *et al.*[1,2] studied emission from thin metallic films and materials coated with metal films, and reported that the single SPP resonance at a bulk metal-vacuum interface is split into two frequencies due to the coupling of SPPs inside the layer, thus affecting the local density of electromagnetic states (LDOS) above the film in vacuum. Similar observations were made by Joulain and Henkel,[3] who discussed the spatial correlation spectrum of near-field thermal radiation above a thin metallic film. Drevillon[4] provided a preliminary study of the near-field spectrum emitted by single and multiple thin films made of polar crystals and metals, without giving detailed physical explanations. This work was extended by Ben-Abdallah *et al.*,[5] who analyzed the possibility of tailoring near-field LDOS spectra above one-dimensional metallodielectric media made of aluminum (Al) and lossless dielectric layers. A target LDOS was prescribed and a genetic algorithm was used to find the best structure, operating in the near ultraviolet, leading to that LDOS profile. While this work showed that it is possible to tune the near-field thermal radiation spectra via multilayered structures, little information is provided about the physical details and on how the interfilm coupling of surface waves affects the LDOS pro-

[a)]Tel.: (859) 257-6336 ext. 80696. FAX: (859) 257-3304. Electronic addresses: mfran0@engr.uky.edu, menguc@engr.uky.edu and pinar.menguc@ozyegin.edu.tr.
[b)]Tel.: +33 (0)4 72 43 88 17. FAX: +33 (0)4 72 43 88 11. Electronic mail: rodolphe.vaillon@insa-lyon.fr.

files calculated. Fu and Tan[6] studied near-field radiative heat transfer between two bulks with one of the material coated with a film supporting SPhPs. They provided extensive parametric analyses of the influence of the coating (material and thickness) on the total radiative heat flux values for TE- and TM-polarized modes both in the near- and far-field regimes; on the other hand, the alteration of the spectral distribution of radiative flux was not investigated. Francoeur *et al.*[7] studied near-field thermal radiation between a silicon carbide (SiC) nanometric film and a bulk, and found a narrow spectral band enhancement of the radiative heat flux due to SPhP coupling inside the layer. Recently, Ben-Abdallah *et al.*[8] investigated near-field radiative heat transfer between two films supporting SPhPs. The authors found that for films of equal thicknesses, the total radiative heat transfer coefficient h_r varies as d^{-2} (where d is the separation gap between the films) as for the case of two bulks, while for layers of different thicknesses, h_r varies as d^{-3}. However, the physical details of this behavior and the spectral variations of h_r as a function of the structure of the system were not systematically addressed.

From the above discussion, it is clear that there is a need to study the physics of near-field emission involving thin layers supporting surface waves. The objective of this paper is therefore to analyze thoroughly the physics of near-field thermal emission by a thin film supporting surface polaritons in the presence of a nonemitting body, also supporting surface waves, in close proximity. This task is accomplished by calculating the LDOS within the gap formed by two SiC films supporting SPhPs in the infrared region. The manuscript is structured as follows: an analytical expression for the LDOS within the gap separating the thin layers is first derived; for this purpose, the Maxwell equations combined with fluctuational electrodynamics are used. Then, the cross-coupled resonant modes for the two film system are investigated via calculation of the dispersion relation. The impact of interfilm coupling on emitted near-field thermal radiation spectra is afterward outlined via computation of the LDOS for various interfilm separation gaps, distances where the fields are observed, and layer thicknesses. Finally, concluding remarks are provided.

II. MATHEMATICAL FORMULATION OF THE LDOS IN THE GAP FORMED BETWEEN TWO THIN FILMS

The geometry considered is schematically depicted in Fig. 1, where a polar (ρ,θ,z) coordinate system is shown.

The media are infinite along the ρ-direction and invariant over θ (i.e., azimuthal symmetry), such that only variations along the z-axis need to be considered. Throughout this paper, it is assumed that the films are in local thermodynamic equilibrium, homogeneous, isotropic, nonmagnetic, and described by a frequency-dependent dielectric function $\varepsilon_r(\omega)$, which is local in space. Also, the surfaces of the layers are considered parallel and perfectly smooth. The two polar crystal films, labeled media 1 and 3 with thicknesses t_1 and t_3, respectively, are submerged in vacuum and separated by a gap of length d_c. Layer 1, at prescribed temperature T_1, emits thermal radiation while medium 3 is assumed to be nonemitting. The thermal radiation field is calculated in the gap at a distance Δ above interface 1-2. The assumption of a nonemitting film is justified by the fact that when calculating radiation transfer between two layers, the energy emitted by one of the media absorbed by the other layer is calculated, and vice versa. The difference between these two values gives the net radiant energy exchanged; therefore, understanding the physics of thermal radiation emission from one film with $T>0$ K, while the other one is nonemitting, allows the interpretation of the realistic case of near-field radiative heat transfer between two emitting films.

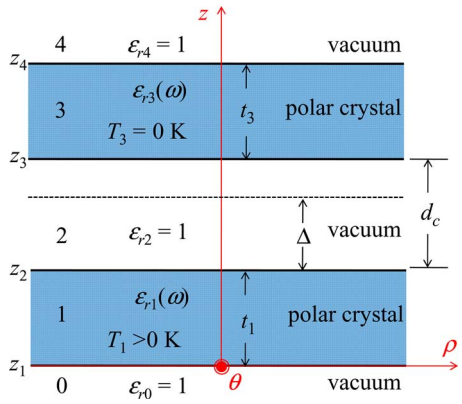

FIG. 1. (Color online) Schematic representation of the geometry considered: The LDOS is calculated at a distance Δ above the emitting film 1 within the gap of thickness d_c.

The emitted near-field thermal radiation spectrum is analyzed via the calculation of the LDOS, which is determined by normalizing the electromagnetic energy density at location Δ by the mean energy of a state $\Theta(\omega,T_1)$. This is justified by the fact that we are investigating the LDOS in the frequency range between 1.5×10^{14} and 1.9×10^{14} rad/s, corresponding to frequencies excited in typical thermal radiation applications involving temperatures between 300 and 2000 K.

The LDOS in the near field is calculated starting from the Maxwell equations combined with fluctuational electrodynamics, where the source of thermal radiation is modeled as a stochastic current density.[19,20] The monochromatic LDOS at location Δ above film 1 in medium 2 can be written as follows after application of the fluctuation-dissipation theorem:

$$\rho_{\omega,12}(\Delta)=\frac{\omega\varepsilon_{r1}''(\omega)}{2\pi^2c_v^2}\int_0^\infty k_\rho dk_\rho\int_{z_1}^{z_2}dz'\times(k_v^2|g_{12m\alpha}^E(k_\rho,\Delta,z',\omega)|^2+|g_{12m\alpha}^H(k_\rho,\Delta,z',\omega)|^2), \quad (1)$$

where the subscripts m and α involve summation over the components ρ, θ, and z. The terms $g_{12m\alpha}^E$ and $g_{12m\alpha}^H$ are the plane wave representation (Weyl components) of the electric and magnetic dyadic Green's functions (DGFs), relating the fields observed at Δ in medium 2 with frequency ω and wavevector k_ρ to a source z' located in layer 1. The electric Weyl representation of the DGF is given by[21]

$$\bar{\bar{\mathbf{g}}}_{12}^{E}(k_\rho,\Delta,z',\omega)=\frac{i}{2k_{z1}}[(A_2^{\mathrm{TE}}\hat{\mathbf{s}}\hat{\mathbf{s}}+A_2^{\mathrm{TM}}\hat{\mathbf{p}}_2^{+}\hat{\mathbf{p}}_1^{+})e^{i[k_{z2}\Delta-k_{z1}z']}+(B_2^{\mathrm{TE}}\hat{\mathbf{s}}\hat{\mathbf{s}}+B_2^{\mathrm{TM}}\hat{\mathbf{p}}_2^{-}\hat{\mathbf{p}}_1^{+})e^{i[-k_{z2}\Delta-k_{z1}z']}+(C_2^{\mathrm{TE}}\hat{\mathbf{s}}\hat{\mathbf{s}}+C_2^{\mathrm{TM}}\hat{\mathbf{p}}_2^{+}\hat{\mathbf{p}}_1^{-})e^{i[k_{z2}\Delta+k_{z1}z']}+(D_2^{\mathrm{TE}}\hat{\mathbf{s}}\hat{\mathbf{s}}+D_2^{\mathrm{TM}}\hat{\mathbf{p}}_2^{-}\hat{\mathbf{p}}_1^{-})e^{i[-k_{z2}\Delta+k_{z1}z']}],\quad(2)$$

where TE- and TM-polarized unit vectors, defined as $\hat{\mathbf{s}}=-\hat{\boldsymbol{\theta}}$ and $\hat{\mathbf{p}}_i^{\pm}=(k_\rho\hat{\mathbf{z}}\mp k_{zi}\hat{\boldsymbol{\rho}})/k_i$, have been used.[22] The magnetic counterpart of Eq. (2) is calculated as $\bar{\bar{\mathbf{g}}}_{12}^{H}=\nabla\times\bar{\bar{\mathbf{g}}}_{12}^{E}$. The coefficients A_2^γ and B_2^γ represent amplitudes of forward (z-positive) and backward (z-negative) traveling waves, respectively, in layer 2 and polarization state γ, arising from a source emitting in the forward direction. Similar explanations hold for C_2^γ and D_2^γ, except that these coefficients arise from a source emitting in the backward direction.[21] Using a transfer matrix approach,[23] the coefficients in medium 2 are given by

$$A_2^\gamma=\frac{e^{ik_{z1}t_1}t_{12}^\gamma}{(1+r_{01}^\gamma r_{12}^\gamma e^{2ik_{z1}t_1})(1-R_1^\gamma R_3^\gamma e^{2ik_{z2}d_c})},\quad(3a)$$

$$B_2^\gamma=R_3^\gamma e^{2ik_{z2}d_c}A_2^\gamma,\quad(3b)$$

$$C_2^\gamma=r_{34}^\gamma A_2^\gamma,\quad(3c)$$

$$D_2^\gamma=r_{34}^\gamma R_3^\gamma e^{2ik_{z2}d_c}A_2^\gamma,\quad(3d)$$

where $r_{j,j+1}^\gamma$ and $t_{j,j+1}^\gamma$ are, respectively, the Fresnel reflection and transmission coefficients at the interface delimiting media j and $j+1$ in polarization state γ, while R_j^γ is the reflection coefficient of layer j in polarization state γ given by[23]

$$R_j^\gamma=\frac{r_{j-1,j}^\gamma+r_{j,j+1}^\gamma e^{2ik_{zj}t_j}}{1+r_{j-1,j}^\gamma r_{j,j+1}^\gamma e^{2ik_{zj}t_j}}.\quad(4)$$

The coefficients given by Eqs. (3a)–(3d) are then included in the electric and magnetic Weyl components of the DGF, which are in turn substituted in Eq. (1). Since SPhPs exist only in TM polarization for nonmagnetic media,[16] we consider strictly the TM evanescent component of the LDOS. After plenty of algebraic manipulations, the following compact expression for the TM evanescent component of the monochromatic LDOS is obtained:

$$\rho_{\omega,12}^{\mathrm{evan,TM}}(\Delta)=\frac{1}{2\pi^2\omega}\int_{k_v}^{\infty}\frac{k_\rho^3dk_\rho}{|k_{z2}|}\frac{\mathrm{Im}(R_1^{\mathrm{TM}})e^{-2k_{z2}''\Delta}}{|1-R_1^{\mathrm{TM}}R_3^{\mathrm{TM}}e^{2ik_{z2}d_c}|^2}\times\left[|1+R_3^{\mathrm{TM}}e^{-2k_{z2}''(d_c-\Delta)}|^2-2\frac{|k_{z2}|^2}{k_\rho^2}\mathrm{Re}(R_3^{\mathrm{TM}})e^{-2k_{z2}''(d_c-\Delta)}\right].\quad(5)$$

Such an analytical expression for the LDOS within the gap between two films has never been reported in literature, and it is therefore important to analyze its physical meaning. The denominator $|1-R_1^{\mathrm{TM}}R_3^{\mathrm{TM}}e^{2ik_{z2}d_c}|^2$ accounts for multiple reflection and wave interference between the two films, while the term in the numerator, $\mathrm{Im}(R_1^{\mathrm{TM}})$, can be seen as the spectral near-field emittance of film 1. The evanescent nature of these modes is also explicitly shown via the exponentially decaying term $e^{-2k_{z2}''\Delta}$. The last term in square bracket on the right-hand side of Eq. (5) accounts for the increase in the emittance of film 1 due to the presence of layer 3. It can be seen via the exponential term $e^{-2k_{z2}''(d_c-\Delta)}$ that the influence of film 3 on the near-field thermal radiation spectrum emitted is maximal when $\Delta=d_c$ and minimal when $\Delta\to0$.

In the limiting case that $d_c\to\infty$, $e^{-2k_{z2}''d_c}\to0$ such that both the denominator and the term in square bracket in Eq. (5) tend to 1. The TM evanescent component of the monochromatic LDOS above a single emitting film is then retrieved as follows:

$$\rho_{\omega,12}^{\mathrm{evan,TM}}(\Delta)=\frac{1}{2\pi^2\omega}\int_{k_v}^{\infty}\frac{k_\rho^3dk_\rho}{|k_{z2}|}\mathrm{Im}(R_1^{\mathrm{TM}})e^{-2k_{z2}''\Delta}.\quad(6)$$

Moreover, if medium 1 is thick (i.e., bulk), then $t_1\to\infty$, $e^{ik_{z1}t_1}\to0$, and $R_1^{\mathrm{TM}}\to r_{21}^{\mathrm{TM}}$. Substitution of $\mathrm{Im}(r_{21}^{\mathrm{TM}})$ in Eq. (6), instead of $\mathrm{Im}(R_1^{\mathrm{TM}})$, provides the LDOS at distance Δ above an emitting bulk as reported by Joulain.[24]

III. RESULTS

A. Dispersion relation of cross-coupled SPhPs

Since medium 1 is at a finite temperature ($T_1\neq0$ K), thermal excitation of transverse optical phonons generate SPhPs at each polar crystal-vacuum interfaces 0-1 and 1-2 with evanescent fields decaying in both media. SPhPs are also excited at interfaces 2-3 and 3-4 of medium 3, but via different mechanisms. SPhPs at interface 2-3 are excited via tunneling of evanescent waves generated by the emitting layer, which is analog to the Otto configuration.[16] At interface 3-4, excitation of SPhPs is done via tunneling of evanescent waves of interface 2-3 through film 3, similar to the Kretschmann configuration.[16] When both T_1 and T_3 are greater than 0 K, SPhP excitation for each layer is due to thermal excitation of charges, as well as excitation via Otto and Kretschmann configurations.

SPhP dispersion relation can be determined by analyzing the resonance condition of the two film system. Resonance arises when $\rho_{\omega,12}^{\mathrm{evan,TM}}\to\infty$. Inspection of Eq. (5) shows that divergence of the TM evanescent component of the monochromatic LDOS can only happen when the following condition is fulfilled:

$$1-R_1^{\mathrm{TM}}R_3^{\mathrm{TM}}\exp(2ik_{z2}d_c)=0.\quad(7)$$

If medium 3 is removed, the TM evanescent component of the LDOS is given by Eq. (6), and $\rho_{\omega,12}^{\mathrm{evan,TM}}\to\infty$ is satisfied when $1-(r_{21}^{\mathrm{TM}})^2\exp(2ik_{z1}t_1)=0$. Solution of this last expression provides the resonant modes of a single film submerged in a given medium. Moreover, if the emitting layer 1 is thick (i.e., bulk), the single resonance condition is given by $r_{21}^{\mathrm{TM}}\to\infty$. Using the definition of the Fresnel reflection coefficient in TM polarization, this condition is fulfilled when $\varepsilon_{r1}k_{z2}+\varepsilon_{r2}k_{z1}=0$, which corresponds to the resonant mode of a single interface delimiting media 1 and 2.[25]

SPhP dispersion relation for the two film system leads to four branches, and is determined by solving Eq. (7) using the

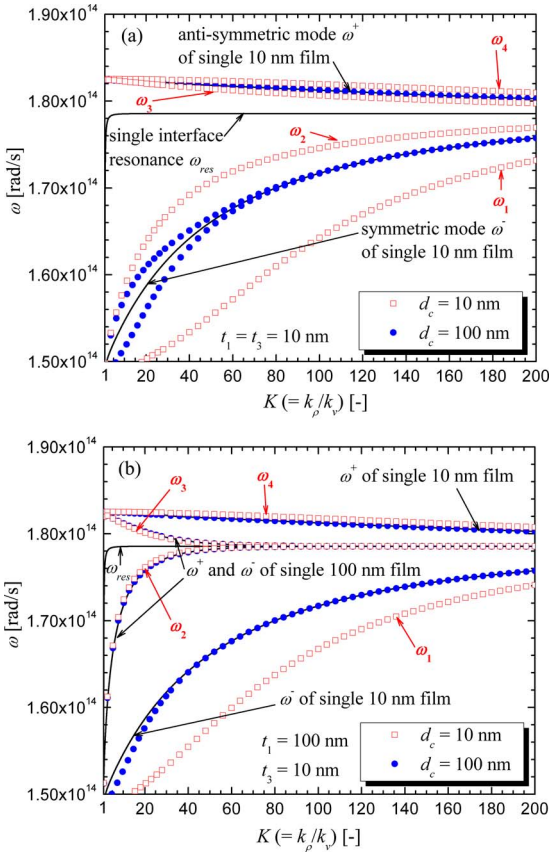

FIG. 2. (Color online) Dispersion relations of SPhPs for t_1 and t_3 thick SiC films submerged in vacuum and separated by a gap d_c: (a) $t_1=t_3=10$ nm, and $d_c=10$ and 100 nm. (b) $t_1=100$ nm, $t_3=10$ nm, and $d_c=10$ and 100 nm. The results are compared with the dispersion relations of single SiC films in vacuum and a single SiC-vacuum interface.

secant method. For the simulations, the dielectric constant of polar crystals is approximated by a damped harmonic oscillator model given by $\varepsilon_r(\omega)=\varepsilon_\infty(\omega^2-\omega_{LO}^2+i\Gamma\omega)/(\omega^2-\omega_{TO}^2+i\Gamma\omega)$, with parameters $\varepsilon_\infty=6.7$, $\omega_{LO}=1.825\times10^{14}$ rad/s, $\omega_{TO}=1.494\times10^{14}$ rad/s, and $\Gamma=8.966\times10^{11}$ 1/s for SiC.[26] Note that the losses are neglected when calculating the dispersion relation (i.e., $\Gamma=0$); the full damped harmonic oscillator is, however, used when computing the LDOS.

In Fig. 2(a), dispersion relations for two 10 nm thick SiC films spaced by a variable d_c of 10 and 100 nm are shown, while SPhP dispersion relations for $t_1=100$ nm, $t_3=10$ nm, and $d_c=10$ and 100 nm are presented in Fig. 2(b). The four branches are identified as a function of their frequencies; the lowest frequency branch is referred to as ω_1, while the highest one is called ω_4. For clarity, this nomenclature is shown in Figs. 2(a) and 2(b) only for $d_c=10$ nm. In both figures, results are compared with the dispersion relations of single SiC films in vacuum and a single SiC-vacuum interface.

In a thin film, the evanescent field of SPhPs associated with each interface can interact with each other, thus leading to a splitting of the SPhP dispersion relation into antisymmetric ω^+ (high frequency) and symmetric ω^- (low frequency) modes.[9–16] The symmetric mode corresponds to the case where the tangential electric field E_ρ has a symmetric distribution with respect to the middle plane of the layer (magnetic fields H_θ at each interface are in phase), and vice versa for the antisymmetric resonance.[15] Comparison of the dispersion relations for 10 and 100 nm thick single SiC films in vacuum shows that the splitting of the resonance becomes more pronounced as the thickness of the film decreases. For large $K(=k_\rho/k_v)$ values, the dispersion relations of both modes approach asymptotically the dispersion curve of a single SiC-vacuum interface. Indeed, the penetration depth of SPhPs in the film is small for large K values. As a consequence, when K is large, the antisymmetric and symmetric branches become degenerate as SPhPs do not couple inside the films, and therefore, the SPhPs at each interface behave independently of each other.[12]

When two films supporting SPhPs are placed in close proximity, further coupling takes place, and the dispersion relation splits into four branches showing antisymmetric and symmetric resonances for each film and for the entire structure.[27,28] This fact is illustrated by analyzing the case $d_c=10$ nm in Fig. 2(a), where both films are 10 nm thick. The modes ω_1 and ω_2 come from the symmetric resonance of each film. The interaction of these symmetric modes in the vacuum gap leads to antisymmetric (ω_2) and symmetric resonances (ω_1) for the whole structure. The antisymmetric resonance ω_2 arises when H_θ oscillations, in phase at the two interfaces of a given layer, are out of phase from one film relative to the other one. Similarly, the symmetric resonance ω_1 due to interfilm coupling arises when H_θ at the four interfaces are in phase. It can be seen in Fig. 2(a) that as d_c increases, ω_1 and ω_2 get closer to the symmetric branch of a single 10 nm thick film submerged in vacuum, since when d_c is large enough, SPhPs on each film behave independently. Similar explanations are applicable to ω_3 and ω_4, which are generated by the coupling of the antisymmetric modes of each film. For the d_c values considered in Fig. 2(a), ω_3 and ω_4 are very close to each other; the proximity effect between the films is more visible for the modes ω_1 and ω_2. For films of different thicknesses [Fig. 2(b)], ω_4 is located above ω^+ of the thinner film (10 nm), and ω_3 is below ω^+ of the thicker film (100 nm). Similar observations can be made for ω_1 and ω_2, which are, respectively, located below and above ω^- of 10 and 100 nm thick films. Note that due to the symmetry of the problem, SPhP dispersion relation for $t_1=10$ nm and $t_3=100$ nm is the same as the one presented in Fig. 2(b). For sufficiently large K values where SPhP coupling is impossible in each layer and between the films, all four branches converge toward the resonant frequency ω_{res} of a single SiC-vacuum interface.

B. LDOS profiles within the gap formed between the two films

The near-field thermal radiation spectrum emitted by film 1 is analyzed by calculating the TM evanescent component of the monochromatic LDOS given by Eq. (5). These LDOS profiles are calculated in the vacuum gap at distance Δ above layer 1, such that when $\Delta=d_c$, this implies that the LDOS is computed just before crossing interface 2-3 (i.e., at $z=z_3^-$). Following the discussion of Sec. III A, the near-field thermal radiation spectrum emitted is expected to be strongly dependent on the parameters t_1, t_3, d_c, and Δ.

At this point, we are making the distinction between the resonant modes of the two film configuration and the "resonance of the LDOS" (or, equivalently, the "resonance of the near-field spectrum"). As discussed in Sec. III A, the resonance of the two film system occurs at all frequencies along the four branches of SPhP dispersion relation. On the other hand, we refer to the resonance of the LDOS as the frequencies maximizing the near-field spectrum emitted. Such resonance of the LDOS can be estimated from SPhP dispersion relation using the following arguments. The LDOS provides a measure of the number of states, or modes, per unit volume and per unit frequency at a given spatial location, and is therefore directly proportional to $|dk_\rho/d\omega|$. As k_ρ increases, the branches of SPhP dispersion relation flatten, thus implying a large $|dk_\rho/d\omega|$ value. We consequently expect the near-field spectrum emitted at Δ to be maximal at the frequencies corresponding to the largest contributing parallel wavevector, $k_{\rho,\max}$, where $|dk_\rho/d\omega|$ is the highest. By estimating the value of $k_{\rho,\max}$ as a function of Δ, it is then possible to evaluate the resonance of the LDOS using SPhP dispersion relation.

The limiting frequencies of LDOS resonance can be determined by performing an asymptotic analysis of SPhP dispersion relation for a single film; these limits are also applicable for the two film configuration. We assume that only evanescent waves with penetration depth in vacuum $\delta_2 \geq \Delta$ contribute to the LDOS calculated at Δ. For a large k_ρ value (i.e., $k_\rho \gg k_v$), the z-component of the wavevector in medium j, strictly defined as $k_{zj}=\sqrt{\varepsilon_{rj}k_v^2-k_\rho^2}$, can be approximated by $k_{zj}\approx ik_\rho$. Using the definition of penetration depth of evanescent waves, $\delta_2 \approx |k_{z2}|^{-1}$, we can write that the largest contributing parallel wavevector to the LDOS is $k_{\rho,\max}\approx\Delta^{-1}$. Substitution of this approximation into the dispersion relation of a single film [given below Eq. (7)] leads to

$$\omega_{\max}^{\pm} \approx \left[\frac{\varepsilon_\infty\omega_{\mathrm{LO}}^2+\omega_{\mathrm{TO}}^2 \mp e^{-t_1/\Delta}(\omega_{\mathrm{TO}}^2-\varepsilon_\infty\omega_{\mathrm{LO}}^2)}{\varepsilon_\infty+1 \mp e^{-t_1/\Delta}(1-\varepsilon_\infty)}\right]^{1/2}, \quad (8)$$

where losses have been neglected in the dielectric function of polar crystals. Equation (8) provides an approximation of the antisymmetric and symmetric resonances of the fields above a single polar crystal film submerged in vacuum as a function of t_1 and Δ. In the limiting case that $t_1 \gg \Delta$, both modes $\omega_{\max}^+$ and $\omega_{\max}^-$ maximizing the LDOS converge toward $\omega_{\mathrm{res}} \approx [(\varepsilon_\infty\omega_{\mathrm{LO}}^2+\omega_{\mathrm{TO}}^2)/(\varepsilon_\infty+1)]^{1/2}$, which is the resonant frequency of a single polar crystal-vacuum interface.[7] The other extreme case arises when $t_1 \ll \Delta$ leading to $\omega_{\max}^+ \approx \omega_{\mathrm{LO}}$, and $\omega_{\max}^- \approx \omega_{\mathrm{TO}}$, limits that prevail regardless of the media surrounding the film. It can be shown that resonance splitting is perceptible on the LDOS profiles for a t_1/Δ value equal or less than unity.

The perturbation of the near-field thermal radiation spectrum emitted by film 1 due to layer 3 is analyzed hereafter as a function of three parameters: the interfilm separation gap d_c, the distance where the fields are calculated Δ, and the thickness of film 3 t_3. The limiting frequencies ω_{TO}, ω_{LO}, and ω_{res} are identified in all figures.

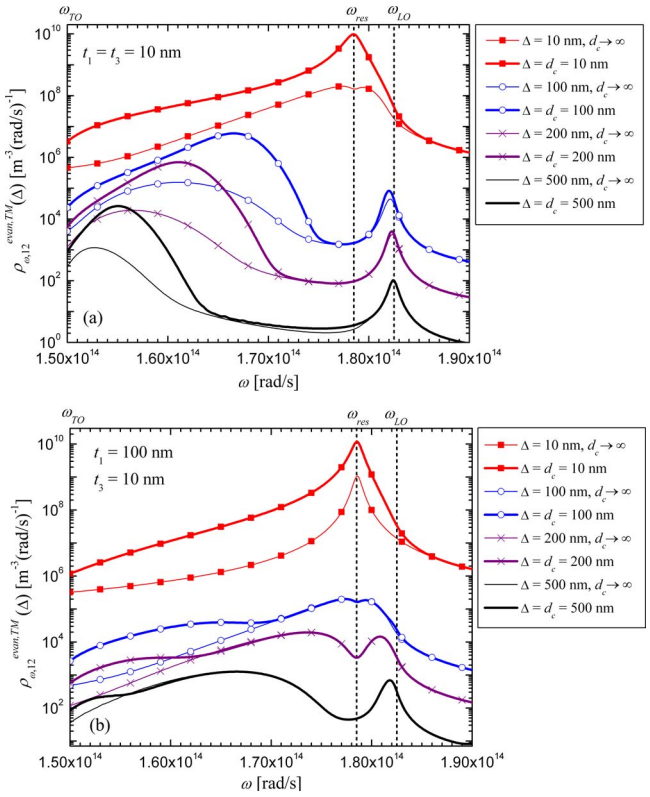

FIG. 3. (Color online) TM evanescent component of the monochromatic LDOS in the gap at $\Delta=d_c=10$, 100, 200, and 500 nm: (a) $t_1=t_3=10$ nm; the results are compared with a single 10 nm thick emitting film. (b) $t_1=100$ nm and $t_3=10$ nm; the results are compared with a single 100 nm thick emitting film.

1. Impact of interfilm distance

LDOS profiles for $d_c=\Delta=10$, 100, 200, and 500 nm are shown in Fig. 3(a) for $t_1=t_3=10$ nm and Fig. 3(b) for $t_1=100$ nm and $t_3=10$ nm. In both cases, for each Δ considered, results are compared with the case $d_c \to \infty$ (i.e., when there is no medium 3).

When there is no film 3, the splitting of the LDOS into two distinct resonant modes is in good agreement with the approximate threshold $t_1/\Delta \leq 1$. As the ratio t_1/Δ decreases below unity, the frequencies maximizing the LDOS clearly converge toward ω_{LO} and ω_{TO}. Physically, the t_1/Δ dependence on the emitted near-field spectrum can be interpreted as follows. For example, when $\Delta=10$ nm in Fig. 3(a), using $k_{\rho,\max}\approx\Delta^{-1}$, the largest contributing $K(K_{\max}=k_{\rho,\max}/k_v)$ value to the LDOS is estimated to be 200. Inspection of the dispersion relation around this approximate limit for a single 10 nm thick film [Fig. 2(a)] reveals that both antisymmetric and symmetric modes have almost reached a plateau where $|dk_\rho/d\omega|$ is very large. As a consequence, even if the portion of dispersion relation below K values of 200 contributes to the LDOS at $\Delta=10$ nm, only the region near $K_{\max}$ can be seen in Fig. 3(a) where $|dk_\rho/d\omega|$ is the highest. As Δ increase, the value of $K_{\max}$ decreases, the gap between ω^+ and ω^- increases, and the near-field thermal radiation spectrum emitted clearly exhibits two distinct resonances. Also, inspection of Figs. 3(a) and 3(b) for small t_1/Δ ratios and $d_c \to \infty$ shows that the LDOS resonance between ω_{res} and ω_{LO} (corresponding to $\omega_{\max}^+$) has a higher degree of spectral co-

herence than the LDOS resonance between ω_{TO} and ω_{res} (corresponding to ω_{max}^{-}), due to greater losses of the symmetric mode.[3]

Figures 3(a) and 3(b) show that the presence of film 3 can enhance significantly emission by layer 1, and perturb slightly the spectral location of the resonance of the LDOS. The enhancement of the LDOS is particularly important for $\Delta=d_c=10$ nm (more than an order of magnitude), in both Figs. 3(a) and 3(b), as strong interfilm SPhP coupling increases the number of electromagnetic modes. For a 10 nm thick emitter and $\Delta=d_c=10$ nm [Fig. 3(a)], the LDOS resonance converges to ω_{res} when medium 3 is present. Figure 2(a) shows that due to SPhP coupling, ω_2 and ω_3 are pushed, respectively, above ω^{-} and below ω^{+}, thus resulting in a maximum LDOS closer to ω_{res} than for a single film. For the 100 nm thick emitter, the resonance of the near-field spectrum emitted is at ω_{res} even for $d_c\to\infty$; the presence of medium 3 at $\Delta=d_c=10$ nm spreads out the resonance over a broader spectral band (i.e., small loss of spectral coherence) as SPhP coupling pushes ω_1 and ω_4, respectively, below ω^{-} and above ω^{+} of a single 10 nm film [see Fig. 2(b)].

As d_c increases, SPhP coupling between the films decreases, and the enhancement of the near-field thermal radiation spectrum emitted by layer 1 consequently decreases. In Fig. 3(a) for $\Delta=d_c=100$, 200, and 500 nm, the presence of film 3 does not alter much the strength and spectral coherence of the LDOS resonance between ω_{res} and ω_{LO} as the antisymmetric mode is not significantly altered by SPhP coupling [see Fig. 2(a) for $d_c=100$ nm]. Medium 3 mostly affects the resonance between ω_{TO} and ω_{res} in terms of LDOS enhancement, spectral location, and broadening. Indeed, for a given d_c value, $|dk_\rho/d\omega|$ is usually larger for ω_2 than ω_1. Since ω_2 is at higher frequencies than ω^{-}, the resonance between ω_{TO} and ω_{res} therefore occurs at a slightly higher frequency when film 3 is present. Similar explanations hold when the emitter is 100 nm thick.

The near-field thermal radiation spectrum emitted by film 1 calculated at $\Delta=d_c$ is always perturbed by the presence of medium 3. Indeed, if the LDOS is greater than zero at $\Delta=d_c$, then SPhPs emitted by film 1 necessarily couple with layer 3 thus affecting the thermal radiation field at Δ.

2. Impact of distance where the LDOS is calculated

To analyze the influence of Δ on the LDOS profiles, we first study the case $t_1=t_3=10$ nm and $d_c=100$ nm already presented in Fig. 3(a) for $\Delta=100$ nm, and calculate the LDOS at two other locations Δ of 10 and 50 nm. In all cases, spectral distributions of the TM evanescent component of the LDOS are compared with those without medium 3; the results are presented in Fig. 4.

Clearly, for Δ values of 10 and 50 nm, the near-field spectrum emitted is only slightly affected by film 3 located at $d_c=100$ nm above film 1. As pointed out earlier, the perturbation of the near-field spectrum emitted by film 1 is mathematically described by the term in square brackets on the right-hand side of Eq. (5), which has a decreasing influence as Δ decreases. Physically, the Δ-dependence can be explained by inspecting SPhP dispersion relation shown in Fig.

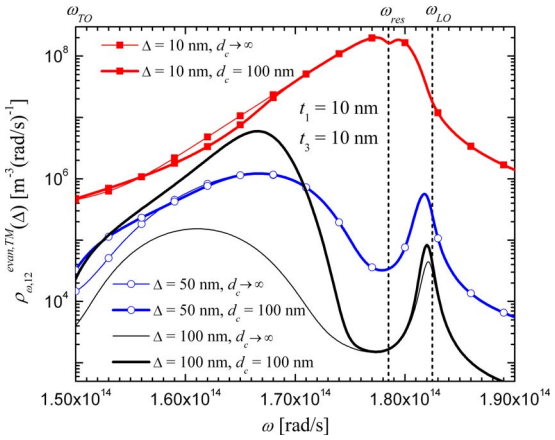

FIG. 4. (Color online) TM evanescent component of the monochromatic LDOS in the gap for $t_1=t_3=10$ nm, $d_c=100$ nm, and $\Delta=10$, 50, and 100 nm; the results are compared with a single 10 nm thick emitting film.

2(a). Using $k_{\rho,max}\approx\Delta^{-1}$, the largest contributing K values to the LDOS (i.e., K_{max}) are estimated to be around 20, 40, and 200 for Δ values of 100, 50, and 10 nm, respectively. As K_{max} increases from 20 to 40, and from 40 to 200, the cross-coupled SPhP modes for the two layer system converge toward ω^{+} and ω^{-} of a single 10 nm thick layer. For large K, the branches of the dispersion relation become flattened, and $|dk_\rho/d\omega|$ takes very large values. Therefore, even if interfilm SPhP coupling arises for lower K values, it does not have a significant influence on the near-field thermal radiation spectrum emitted by film 1 at $\Delta\ll d_c$ as the LDOS is dominated by SPhPs, with small penetration depths, that do not couple with the modes of the nonemitting film.

LDOS profiles are reported in Fig. 5 for t_1 and t_3 fixed, respectively, at 100 and 10 nm, $\Delta=50$ nm, and interfilm distances d_c of 50, 70, 100, and 500 nm; the results are compared with the case of a single emitting film. Moreover, the TM evanescent component of the monochromatic LDOS per unit wavevector k_ρ is reported for the aforementioned configuration with $d_c=50$ nm in Fig. 6(a), and for $d_c=100$ nm in Fig. 6(b); SPhP dispersion relations are also plotted in these figures.

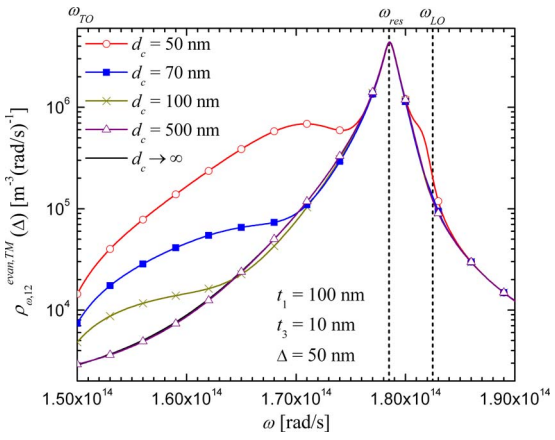

FIG. 5. (Color online) TM evanescent component of the monochromatic LDOS in the gap for $t_1=100$ nm, $t_3=10$ nm, $\Delta=50$ nm, and $d_c=50$, 70, 100, and 500 nm; the results are compared with a single 100 nm thick emitting film.

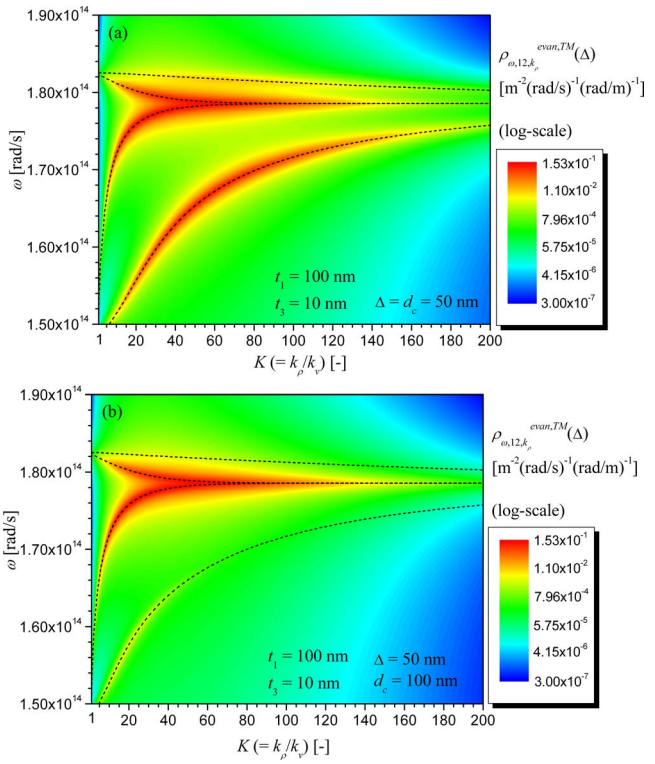

FIG. 6. (Color online) TM evanescent component of the monochromatic LDOS per unit k_ρ (in log scale) in the gap for $t_1=100$ nm, $t_3=10$ nm, and $\Delta=50$ nm: (a) $d_c=50$ nm. (b) $d_c=100$ nm.

In Fig. 5, regardless of the value of d_c, the maximum LDOS is always located at ω_{res} since for $\Delta=50$ nm, K_{max} is estimated around 40 where the modes ω_2 and ω_3 have almost reached a plateau. As d_c decreases from 100 to 50 nm, LDOS resonance between ω_{TO} and ω_{res} shifts toward higher frequencies. Indeed, as d_c decreases, coupling between the films becomes stronger and arises for SPhPs with lower penetration depths (i.e., larger K values), such that the resonance shifts toward higher frequencies where $|dk_\rho/d\omega|$ is large.

Figure 6(a) for $d_c=\Delta=50$ nm shows clearly that film 3 enhances near-field radiation emission around the four branches of the dispersion relation. Emission is, however, much stronger around ω_{res}, where the density of electromagnetic modes is large (i.e., where $|dk_\rho/d\omega|$ is flat). When d_c increases to 100 nm [Fig. 6(b)], the resonance at ω_{res} is still present, while the enhancement of the LDOS due to interfilm coupling has significantly decreased. It is worth noting that K_{max} estimated using $k_{\rho,max}\approx\Delta^{-1}$ is smaller than what is shown in Figs. 6(a) and 6(b). To derive this approximation, we have used the definition of penetration depth of evanescent waves as $\delta_j\approx|k_{zj}|^{-1}$, which corresponds to the distance from the interface where the field amplitude has decayed to e^{-1} of its value. Therefore, while $k_{\rho,max}\approx\Delta^{-1}$ combined with SPhP dispersion relations can be used to explain the LDOS profiles, this procedure cannot predict with great accuracy the spectral locations of the resonant modes maximizing the near-field spectrum emitted. Such predictions, beyond the scope of this paper, would require a modification of the value of δ.

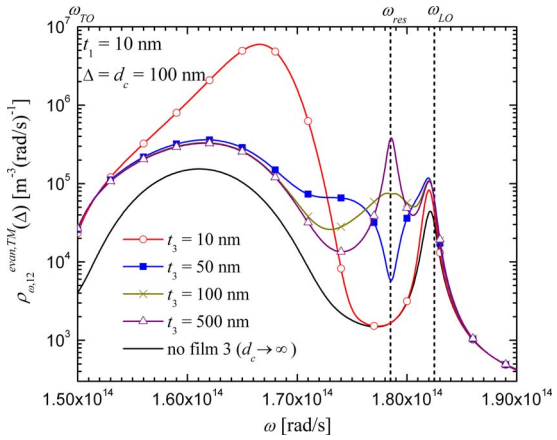

FIG. 7. (Color online) TM evanescent component of the monochromatic LDOS in the gap for $t_1=10$ nm, $\Delta=d_c=100$ nm, and $t_3=10$, 50, 100, and 500 nm; the results are compared with a single 10 nm thick emitting film.

3. Impact of thickness of film 3

The TM evanescent component of the monochromatic LDOS is shown in Fig. 7 for $t_1=10$ nm, $\Delta=d_c=100$ nm, and varying t_3 values of 10, 50, 100, and 500 nm; the results are compared with the case when there is no film 3.

Regardless of the value of t_3, near-field thermal radiation emission is enhanced when film 3 is present compared to the case $d_c\rightarrow\infty$. As t_3 increases, the spectral distributions of LDOS in TM polarization vary significantly. Indeed, when the thickness of medium 3 increases, the modes ω_2 and ω_3 converge toward ω_{res} for lower K values, while ω_1 and ω_4 are only slightly affected; this can be seen by comparing SPhP dispersion relations of Figs. 2(a) and 2(b) for $d_c=100$ nm. Therefore, it can be seen in Fig. 7 that as t_3 increases, the LDOS also increases around ω_{res}. When $t_3=500$ nm, a resonant peak clearly emerges at ω_{res} as the modes ω_2 and ω_3 converge to ω_{res} for very small K values, since SPhP coupling in a 500 nm thick medium is weak.

IV. CONCLUSIONS

The physics of near-field thermal radiation emission by a thin layer supporting surface polaritons, in the presence of a nonemitting film also supporting surface waves, has been analyzed. This was accomplished by calculating the TM evanescent component of the monochromatic LDOS within the gap formed between two SiC films supporting SPhPs in the infrared region.

An analytical expression for the LDOS in the gap between two films has been presented for the first time. The equation has shown that due to SPhP coupling within and between the layers, the dispersion relation splits into four resonant cross-coupled modes. The analysis of the equation has also revealed that thermal emission by a film increases due to the presence of a second nonemitting layer.

The impact of interfilm separation gap d_c, the distance where the fields are calculated Δ, and the thickness of the nonemitting film t_3 on the LDOS profiles have been analyzed. When Δ and d_c were of equal lengths, the results have shown that thermal emission can significantly increase solely due to the presence of a nonemitting layer supporting SPhPs

(more than an order of magnitude for $d_c=10$ nm). This perturbation is due to SPhP coupling between the films, which increase the number of available electromagnetic modes, while decreasing the spectral coherence of LDOS resonance. The results have revealed that the low frequency modes are mostly affected by this loss of spectral coherence. For a fixed configuration, it has been shown that as Δ decreases below d_c, the near-field spectrum is no longer affected by the presence of a second nonemitting film, since the LDOS is dominated by SPhPs with large parallel wavevectors (i.e., small penetration depths) that do not couple with the nonemitting medium. Finally, it has been shown that spectral distributions of LDOS are significantly altered as the thickness of the nonemitting film increases relative to the thickness of the emitter. This is due to the fact that as t_3 increases, a magnifying mismatch between the cross-coupled SPhP modes leading to a maximum LDOS develops, thus resulting in different spectra, which are highly dependent on the value of t_3.

It is worth noting that for thin films, spatial dispersion of the dielectric function of the materials might be important, and consequently nonlocal effects will be investigated in a future research effort. Moreover, when applying the fluctuational electrodynamics theory, the media are assumed to be in local thermodynamic equilibrium. For films with thicknesses of the order of few nanometers, this assumption might be questionable. On the other hand, this theory, built on macroscopic electrodynamics, is currently the only tool available to treat near-field thermal radiation emission. Validation of the application of fluctuational electrodynamics to very thin layers should come from experiments.

The work presented here provides guidelines on how near-field thermal radiation emission by a film is affected by the presence of another body. Starting from this physical analysis, we aim to develop an engineering approach to tune near-field thermal radiation emission via multilayered media, without necessarily going through complex inversion procedures, which will be applied to design optimal nanoscale-gap TPV power generators.

ACKNOWLEDGMENTS

This work is partially sponsored by the U.S. Department of Energy Grant No. DE-FG02-07ER46375 and the Kentucky Science and Engineering Foundation Grant No. KSEF-1718-RDE-011. Partial support for M.P.M. is received from the FP-7-PEOPLE-IRG-2008 Grant No. 239382 at Ozyegin University.

[1] S.-A. Biehs, D. Reddig, and M. Holthaus, Eur. Phys. J. B **55**, 237 (2007).
[2] S.-A. Biehs, Eur. Phys. J. B **58**, 423 (2007).
[3] K. Joulain and C. Henkel, Appl. Phys. B: Lasers Opt. **93**, 151 (2008).
[4] J. Drevillon, Ph.D. thesis, Université de Nantes, 2007.
[5] P. Ben-Abdallah, K. Joulain, J. Drevillon, and G. Domingues, Appl. Phys. Lett. **94**, 153117 (2009).
[6] C. J. Fu and W. C. Tan, J. Quant. Spectrosc. Radiat. Transf. **110**, 1027 (2009).
[7] M. Francoeur, M. P. Mengüç, and R. Vaillon, Appl. Phys. Lett. **93**, 043109 (2008).
[8] P. Ben-Abdallah, K. Joulain, J. Drevillon, and G. Domingues, J. Appl. Phys. **106**, 044306 (2009).
[9] K. L. Kliewer and R. Fuchs, Phys. Rev. **144**, 495 (1966).
[10] K. L. Kliewer and R. Fuchs, Phys. Rev. **150**, 573 (1966).
[11] K. L. Kliewer and R. Fuchs, Phys. Rev. **153**, 498 (1967).
[12] E. N. Economou, Phys. Rev. **182**, 539 (1969).
[13] D. Sarid, Phys. Rev. Lett. **47**, 1927 (1981).
[14] J. J. Burke, G. I. Stegeman, and T. Tamir, Phys. Rev. B **33**, 5186 (1986).
[15] J. Dionne, L. A. Sweatlock, H. A. Atwater, and A. Polman, Phys. Rev. B **72**, 075405 (2005).
[16] S. A. Maier, *Plasmonics: Fundamentals and Applications* (Springer, New York, 2007).
[17] M. Laroche, R. Carminati, and J.-J. Greffet, J. Appl. Phys. **100**, 063704 (2006).
[18] K. Park, S. Basu, W. P. King, and Z. M. Zhang, J. Quant. Spectrosc. Radiat. Transf. **109**, 305 (2008).
[19] S. M. Rytov, Y. A. Kravtsov, and V. I. Tatarski, *Principles of Statistical Radiophysics* (Springer-Verlag, Berlin, 1987), Vol. 3.
[20] M. Francoeur and M. P. Mengüç, J. Quant. Spectrosc. Radiat. Transf. **109**, 280 (2008).
[21] M. Francoeur, M. P. Mengüç, and R. Vaillon, J. Quant. Spectrosc. Radiat. Transf. **110**, 2002 (2009).
[22] J. E. Sipe, J. Opt. Soc. Am. B **4**, 481 (1987).
[23] P. Yeh, *Optical Waves in Layered Media* (Wiley, Hoboken, NJ, 2005).
[24] K. Joulain, *Topics in Applied Physics: Microscale and Nanoscale Heat Transfer* (Springer, Berlin, 2007), Vol. 107, p. 107.
[25] K. Joulain, J.-P. Mulet, F. Marquier, R. Carminati, and J.-J. Greffet, Surf. Sci. Rep. **57**, 59 (2005).
[26] E. D. Palik, *Handbook of Optical Constants of Solids* (Academic, San Diego, CA, 1998), Vol. 1.
[27] M. A. Gilmore and B. L. Johnson, J. Appl. Phys. **93**, 4497 (2003).
[28] J. Chen, G. A. Smolyakov, S. R. J. Brueck, and K. J. Malloy, Opt. Express **16**, 14902 (2008).